DIRECT NUMERICAL SIMULATION OF DOUBLE DIFFUSIVE NATURAL CONVECTION IN A CLOSED MIXTURE CAVITY HEATED FROM BELOW

by

Yaowen XIA[a,b*] and Juan CHEN[b]

[a] Education Ministry Key Laboratory of Advanced Technology and Preparation for Renewable Energy Materials, Kunming, Yunnan, China
[b] School of Information Science and Technology, Yunnan Normal University, Kunming, China

Original scientific paper
https://doi.org/10.2298/TSCI221107069X

Double diffusive natural convection is one of the most widely used study subjects in heat and mass transfer. In this present study, double diffusive natural convection heating from below the wall in a closed cavity was studied with direct numerical simulation method. The flow characteristics are presented as isotherms, iso concentrations, and streamlines. The results show that Ra_T has signification strong effects on average Nusselt number, with a more considerable Ra_T, the value of Nusselt number more higher. These were also found to increase with increasing buoyancy ratio for adding flow and decrease as buoyancy ratio decreases for opposing flows.

Key words: *double diffusive natural convection, heat and mass transfer, buoyancy ratio, direct numerical simulation*

Introduction

In nature and environmental settings, a closed cavity heated from below contain two (or more) scalar components which contribute to their density, predominantly temperature and concentration [1, 2]. Double diffusive convection (DDC) is coexistent the effect of temperature and concentration, which has been studied extensively. It has been adapted in various fields such as oceanography, astrophysics, geology, metallurgy [3, 4], crystal growth reactor [5], nuclear waste storage [6], and dispersion of pollutants indoors [7].

There have been numerous studies on DDC, and many scholars performed experimentally and numerical studies of the thermosolutal convection under combined the effect of temperature and concentration [8-12]. It also developed a series of quantitative dimensionless heat and mass transfer rates under the consideration of assisting or opposing buoyancy.

Many numerical methods tools, including the finite different method (FDM), finite volume method (FVM), finite element method (FEM), and lattice Boltzmann method (LBM), are used to study on DDC. Chen *et al.* [13] investigated the DDC using LBM method, and analyzed the key physical parameters affecting heat and mass transfer characteristics. Corcione *et al.* [14] numerically investigated the DDC in vertical square enclosures combined the effect of temperature and concentration based on the SIMPLE C algorithm. The numerical results were used to found the correlation for the Nusselt numbers of the enclosure cavity. Xu

* Corresponding author, e-mail: yaowenxia@ynnu.edu.cn

et al. [15, 16] used LBM method to study the DDC around the heating cylinder in the square shell. Nia *et al.* [17] conducted a numerical analysis of the radiation gas-flow with coexistence of temperature and concentration in a square cavity.

The DDC related stability, MHD, also was the attention of the researchers. The stability DDC combined the effect of temperature and concentration difference was analyzed, and rotation stabilizes diffusion convection cause instability [18-20]. The influences of MHD on DDC in cavities have been studied by many researchers [21-23].

The structural stability of Brinkman-Forchheimer model of DDC has also been reported in the new documents. Ali *et al.* [24] and Meften *et al.* [25] gave the continuous dependence and symmetric results of solutions of Brinkman-Forchheimer equations with a variable viscosity with the aid of some a priori estimates.

The large eddy simulation (LES) and direct numerical simulation (DNS) in the closed cavity were also used to study DDC. Chen *et al.* [26, 27] used the LES model to investigate DDC, and obtained the quantitative relations between the average Nusselt number, Nu_m, the buoyancy ratio, N, and the thermal Rayleigh number, Ra_T, parameters. Wang [28] numerically studied the DDC using the FVM. Nee *et al.* [29] investigated the 3-D DDC, showing that the LBM-FDM was better than FDM.

Carpenter *et al.* [30] evolved the double diffusive interface using DNS. They analyzed the double diffusive instability due to density difference induced temperature and concentration gradient buoyancy. The DNS-DDC model is derived to predict the flow patterns in the rectangular cavity by Liang *et al.* [31]. Penney *et al.* [32] present three DNS of laboratory scale double diffusive gravity currents.

It is important to note that humans generate an abundance of CO_2 indoors. Heat and air quality assessments that use air-CO_2 mixtures as working fluids entering buildings, even for healthcare purposes, must therefore, be studied in depth [33]. Serrano-Arellano *et al.* [7] numerical investigate DDC of air-CO_2 mixture in a square cavity. It was noticed that the buoyancy ratio effect on heat transfer depended on the location of the high CO_2 source. Serrano Arellano *et al.* [34] studied natural thermosolutal convection for the same parameters cavity. It was found that convection and heat transfer amounts increase with the mass transfer under consideration. However, it decreases with thermal Rayleigh increases. Nikbakhti *et al.* [35] deal with the DDC in a closed cavity partially heated vertical walls. It was extended by Nikbakhti *et al.* [36] using numerically performed an investigation of DDC inside a cavity. In addition, they also analyzed the heat and mass characteristics depending on the import factors, which includes the orientation of the temperature and concentration buoyancy forces. The effect of non-gray gas radiation on DDC in the square enclosure is studied numerically by Benbrik *et al.* [37]. It is obtained that the radiative effects on double diffusive convex on more critical for air-H_2O mixtures than for air-CO_2 ones. Alhusseny *et al.* [38] numerically analysed DDC with constant vertical wall but different concentration and insulated horizontal walls in long rotating porous channels. It was noticed that heat and mass characteristics is reduced due to an increase in the rotation strength. Khalaf *et al.* [39] performed DDC for staggered cavities thermal Rayleigh number over $10^4 \le Ra_T \le 10^6$, buoyancy ratio over $-5 \le N \le 5$, Lewis number, over $1.0 \le Le \le 5.0$, and aspect ratio, A, over $0.1 \le A \le 0.2$.

According to the aforementioned literature, most numerical studies related to DDC use FDM, FVM, FEM, and LBM. However, to our knowledge, there has little research on DDC with an air-CO_2 mixture in a room fluid using DNS.

Methodology

Problem formulation

As shown in fig. 1, the physical and its numerical model can be simplified into a 2-D rectangular domain with height H (2.48 m) and width W (5.89 m). The working fluid, in this case, is an air-CO_2 mixture. The air-CO_2 mixture in the room is Newtonian, stationary at a constant temperature of T_a and a constant CO_2 concentration of C_a. The bottom wall is isothermal with T_H, the left, right, and top walls are assumed to be both T_C. The highest CO_2 concentration C_H can be located on the bottom wall or other walls depending on the buoyancy ratio, and CO_2 concentration values vary with N. The lowest CO_2 concentration is assumed to be constant (C_L = 350 ppm).

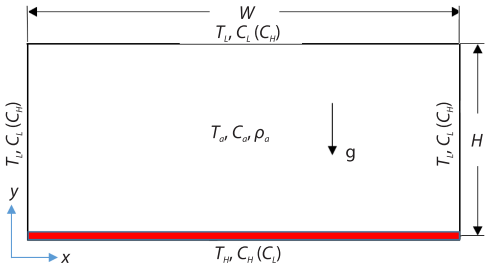

Figure 1. The sketch of physical and numerical model

Governing equations, initial and boundary conditions

The corresponding momentum, energy, and pollutant mass species conservation equation, which use the Oberbeck-Boussinesq approximation for buoyancy and gravity acting in the negative Y (vertical) direction, control the flow of air-CO_2 contaminants in the room. The equations are written in the co-ordinate system:

$$\frac{\partial U}{\partial X}+\frac{\partial V}{\partial Y}=0 \tag{1}$$

$$\frac{\partial U}{\partial t}+\frac{\partial (UU)}{\partial X}+\frac{\partial (VU)}{\partial Y}=-\frac{1}{\rho}\frac{\partial P}{\partial X}+\nu\left(\frac{\partial^2 U}{\partial X^2}+\frac{\partial^2 U}{\partial Y^2}\right) \tag{2}$$

$$\frac{\partial V}{\partial t}+\frac{\partial (UV)}{\partial X}+\frac{\partial (VV)}{\partial Y}=-\frac{1}{\rho}\frac{\partial P}{\partial Y}+\nu\left(\frac{\partial^2 V}{\partial X^2}+\frac{\partial^2 V}{\partial Y^2}\right)+\rho\left[\beta_T (T-T_a)+\beta_C (C-C_a)\right] \tag{3}$$

$$\frac{\partial T}{\partial t}+\frac{\partial (UT)}{\partial X}+\frac{\partial (VT)}{\partial Y}=\kappa\left(\frac{\partial^2 T}{\partial X^2}+\frac{\partial^2 T}{\partial Y^2}\right) \tag{4}$$

$$\frac{\partial C}{\partial t}+\frac{\partial (UC)}{\partial X}+\frac{\partial (VC)}{\partial Y}=D\left(\frac{\partial^2 C}{\partial X^2}+\frac{\partial^2 C}{\partial Y^2}\right) \tag{5}$$

The Oberbeck-Boussinesq approximation is applied here, whereby fluid density at temperature, T, and concentration, C, is computed:

$$\rho(T,C)=\rho_a (T_a,C_a)\left[1-\beta_T (T-T_a)-\beta_C (C-C_a)\right] \tag{6}$$

The initial conditions are $T = T_a$ and $C = C_a$ everywhere in the numerical domain, except at the bottom wall is $\theta = 0.5$, at other boundary walls are $\theta = –0.5$. The CO_2 concentrations specified on the vertical and horizontal walls are $\phi = 0.5$ at $y = 0$, $y = 1$, $x = 0$, and $\phi = –0.5$ or $\phi = 0.5$ at $x = 2.375$, respectively.

The dimensionless forms of the corresponding governing equations can be written:

$$\frac{\partial u}{\partial x}+\frac{\partial v}{\partial y}=0 \tag{7}$$

$$\frac{\partial u}{\partial \tau}+u\frac{\partial(u)}{\partial x}+v\frac{\partial(u)}{\partial y}=-\frac{\partial p}{\partial x}+\mathrm{Pr}\left(\frac{\partial^2 u}{\partial x^2}+\frac{\partial^2 u}{\partial y^2}\right) \tag{8}$$

$$\frac{\partial v}{\partial \tau}+u\frac{\partial(v)}{\partial x}+v\frac{\partial(v)}{\partial y}=-\frac{\partial p}{\partial y}+\mathrm{Pr}\left(\frac{\partial^2 v}{\partial x^2}+\frac{\partial^2 v}{\partial y^2}\right)+\mathrm{Pr}(\theta+N\phi) \tag{9}$$

$$\frac{\partial \theta}{\partial \tau}+u\frac{\partial(\theta)}{\partial x}+v\frac{\partial(\theta)}{\partial y}=a\left(\frac{\partial^2 \theta}{\partial x^2}+\frac{\partial^2 \theta}{\partial y^2}\right) \tag{10}$$

$$\frac{\partial \phi}{\partial \tau}+u\frac{\partial(\phi)}{\partial x}+v\frac{\partial(\phi)}{\partial y}=Sc\left(\frac{\partial^2 \phi}{\partial x^2}+\frac{\partial^2 \phi}{\partial y^2}\right) \tag{11}$$

in which the dimensionless parameters are obtained

$$x=\frac{X}{H},\quad y=\frac{Y}{H},\quad u=\frac{U}{V_0},\quad v=\frac{V}{V_0}$$

$$\tau=\frac{t}{\frac{X}{V_0}},\quad p=\frac{P}{\rho_0 V_0^2},\quad \theta=\frac{T-T_0}{T_H-T_L},\quad \phi=\frac{C-C_0}{C_H-C_L}$$

where T_0 and C_0 are reference temperatures and concentrations and α is thermal diffusivity.

The Schmidt number and buoyancy ratio N are defined:

$$\mathrm{Sc}=\frac{\nu}{D},\ N=\frac{\beta_C(C_a-C_0)}{\beta_T(T_a-T_0)} \tag{12}$$

where N is the relative contribution of temperature and concentration density..

The average Nusselt number, Nu_m, is usually used to quantify heat transfer characteristics [40]:

$$\mathrm{Nu}_m=\int_0^1(\mathrm{Nu}_L)_{X=0}\mathrm{d}Y=\int_0^1\left(-\frac{\partial\theta}{\partial X}\right)_{X=0}\mathrm{d}Y \tag{13}$$

Mesh and benchmarking of DNS

In order to ensure that the DNS is independent of the grid and time step, many grids and time step independent tests were carried out. In this study, It chose the specific case of Pr = 0.71, $\mathrm{Ra}_T = 7.0 \cdot 10^9$, Le = 1.0, $N = -1$, which presents the horizontal profiles of velocity and temperature at $x = 0.5$, and the vertical profile of velocity and temperature at $y = 0.5$, all at $t = 10$ seconds, as shown in fig. 2. These results were obtained with three meshes 1200 × 500 (0.5983 million cells), 1500 × 700 (1.0478 million cells), 1800 × 750 (1.3475 million cells), and three-time steps of 1 second, 0.5 second, and 0.25 second. It clear that the DNS results obtained by using three different meshes with the same time steps of 0.5 second are essentially the same. The comparison of the DNS results obtained by using three different time steps within the same mesh of 1.0478 million cells, as shown in fig. 2, clearly shows that the differences are very insignificant. All DNS runs in the current investigation employed the mesh with 1.0478 million grids and a time step of 0.5 second because it was determined that these parameters could provide numerical simulation results that were sufficiently accurate.

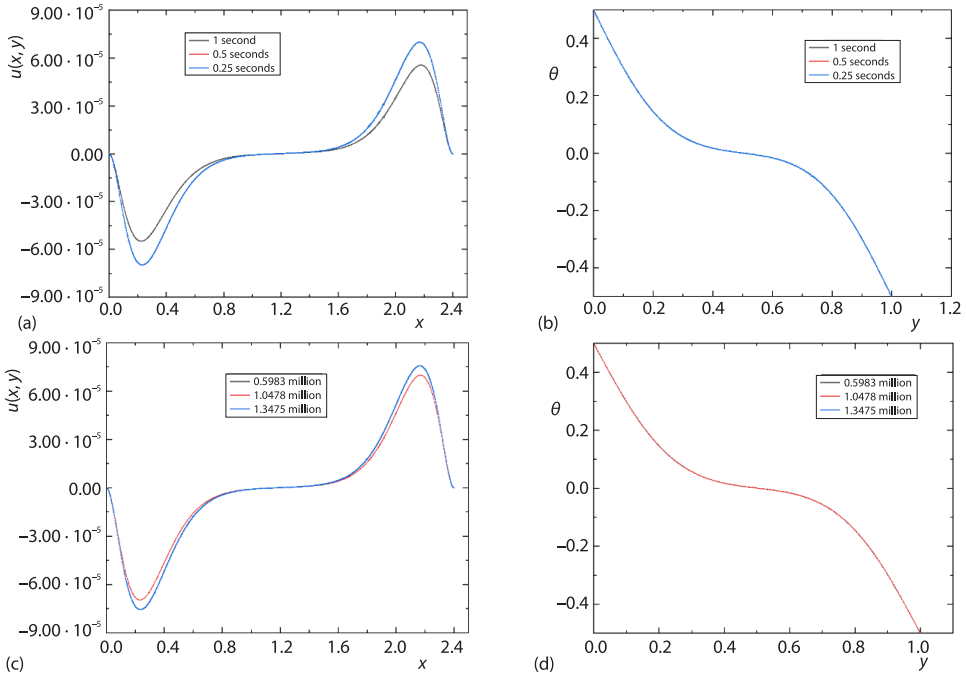

Figure 2. Comparisons between the DNS results from three different steps (a) and (b), three different meshes (c) and (d), *u*-velocity (a) and (c), and temperature (b) and (d)

The 2-D transient model established physical and mathematical model of DDC in a closed mixture cavity heating from below under the combined effect of temperature and concentration forces, and introduced user-defined function of fluid density. By means of user-defined functions introduced concentration transport equation is established at the same time. The numerical results are compared with the results in the documents and to ensure the numerical simulations' accuracy. It is now well acknowledged that a numerical code requires validation and verification of the outcomes using the data at hand. We chose the focus of several numerical validations to benchmark the code utilized in the current investigation [8, 10, 41, 42]. The following parameters were used: $\mathrm{Pr} = 0.71$, $\mathrm{Ra}_T = 1.0 \cdot 10^7$, $\mathrm{Le} = 1.0$, gathers the values of Nu_m. The excellent agreement demonstrates the reasonable accuracy of ANSYS FLUENT code for direct numerical simulating DDC in a closed mixture cavity heated from below in the present study.

Results and discussion

The fluid for DNS runs in present study is air-CO_2 mixture fluid, with density ρ_a =1.16 kg/m^3, kinematic viscosity $\nu = 1.85 \cdot 10^{-3}$ m^2/s, thermal expansion coefficient $\beta_T = 3.33 \cdot 10^3$ 1/K, concentration expansion coefficient $\beta_T = -0.34$ 1/%, Pr = 0.71, Le = 1.0, Ra_T over $10^4 \leq \mathrm{Ra}_T \leq 2 \cdot 10^7$, N over $-5 \leq N \leq +5.0$, respectively.

Qualitative observation

Evolution of a typical thermosolutal natural convection

The indoor air moves irregularly with effect of temperature and CO_2 concentration, as shown in fig. 3. The density of indoor air decreases due to the floor heating and more significant CO_2 concentration, and the indoor air becomes upward. It found that the left, right, and top

walls are low temperatures and CO_2 concentrations. The indoor air moves up along the horizontal axis to the top, then flows down along the vertical walls, mixed with the upwelling air under the negative buoyancy due to the temperature and CO_2 concentration effect. Two circulations in the room flow come out one counterclockwise and one clockwise vortex. The indoor temperature and CO_2 concentration stay stable after $\tau = 747$ to form the highest temperature and largest CO_2 concentration in the axis area, lowest temperature and lowest CO_2 concentration in the left vertical, right vertical and floor walls. The indoor comfort areas are located in the centre of the rooms, meeting the work area comfortably.

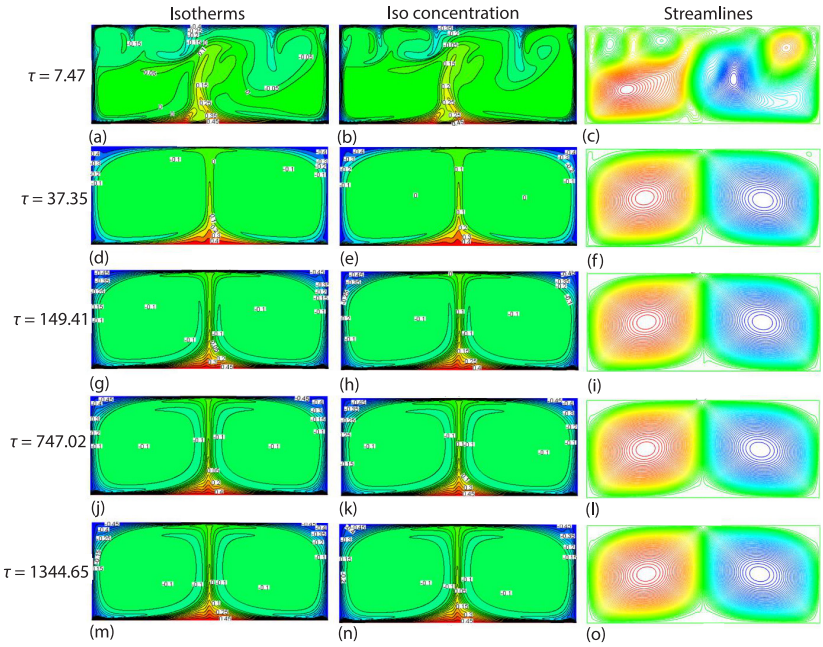

Figure 3. Time series of dimensionless isothermal (a), (d), (g), (j), and (m), iso-concentrations (b), (e), (h), (k), and (n), and streamlines (c), (f), (i), (l), and (o) for the case of $Ra_T = 1.0 \cdot 10^7$, Pr = 0.71, Le = 1.0, and $N = -1.0$

The influence of thermal Rayleigh number

Figure 4 presents the snapshots of the isothermal, iso concentrations, and streamlines for the case of $1.0 \cdot 10^4 \leq Ra_T \leq 2.0 \cdot 10^7$, Pr = 0.71, Le = 1.0, and $N = 1.0$. It is found that N is a positive thermosolutal buoyancy force that is cooperative, is conducive to heat and mass transfer. It was showed that the room temperature and CO_2 concentration were linearly stratified at the fully developed stage, with higher temperature and concentration in the lower part of a room and upper part in lower temperature and concentration. From this figure, it is seen that when Ra_T increase, both temperature lines and concentrations lines become denser, and the stagnation zone of the left and the right wall becomes smaller, as shown in figs. 4(j)-4(l). Indoor air is clearly shown to move upward, and the temperature and CO_2 concentration in the top area of the room is due to the effect of floor heating, hence prolonging the time of stability in the room.

Figure 5 presents the snapshots of the isothermal, iso concentrations, and streamlines for the case of $1.0 \cdot 10^4 \leq Ra_T \leq 2.0 \cdot 10^7$, Pr = 0.71, Le = 1.0, and $N = -1.0$. It is found that the

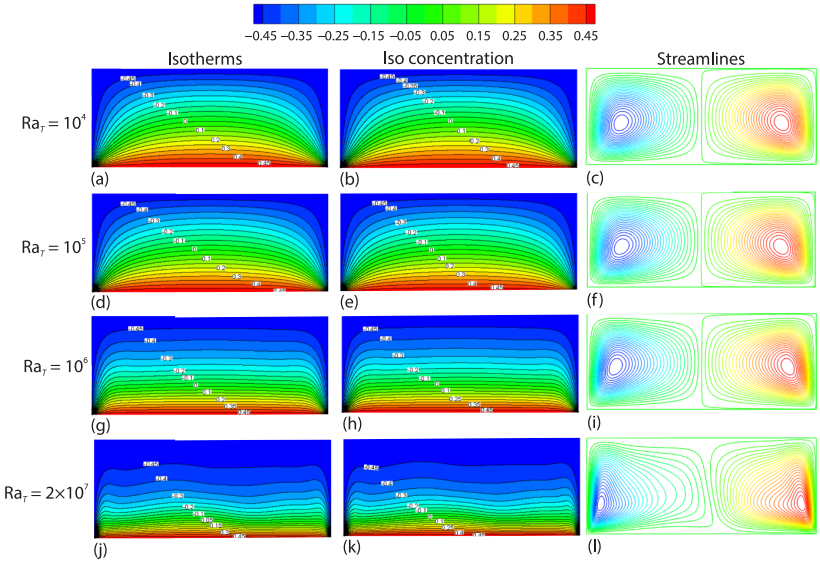

Figure 4. Dimensionless isothermal (a), (d), (g) and (j), iso concentrations (b), (e), (h), and (k), and streamlines (c), (f), (i), and (l) varying at different Ra_T at $N = 1.0$

room temperature and CO_2 concentration were also linearly stratified at the fully developed stage, the lower part of the room is higher temperature and lower concentration, and the upper part is a lower temperature and more significant concentration. It can also observe that when Ra_T increase, both temperature lines and concentrations lines become denser, and the stagnation zone of the vertical walls becomes smaller, as shown in figs. 5(j)-5(l). Furthermore, compared with fig. 4, temperature lines and concentrations lines are sparse, the stratified area becomes more prominent. The reduction of temperature, concentration and velocity, buoyancy forces combined the effect of temperature and CO_2 concentration intensifies the heat and mass transfer.

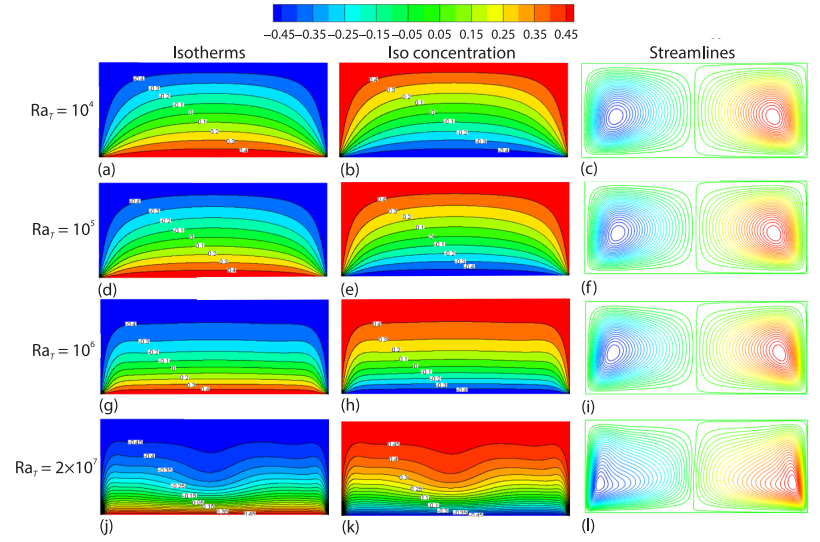

Figure 5. Dimensionless isothermal (a), (d), (g), and (j), iso-concentrations (b), (e), (h), and (k), and streamlines (c), (f), (i), and (l) varying at different Ra_T at $N = -1.0$

The flow in the bottom heating cavity increases gradually as the Ra_T number increase, eventually forming fluctuation of flow inside the cavity. At low Ra_T number, fluid viscosity is significant, with slow flow development, clear indoor temperature and concentration stratification, and smooth and evenly changed curve. The DDC at high Ra_T number develops rapidly, longitudinal slope of curve changes greatly, and local irregularity fluctuates along longitudinal direction. It indicates that DDC becomes intense, transient characteristics are more obvious, and turbulence instability occurs with Ra_T number increases.

Indeed, the movement exhibits one counterclockwise and one clockwise vortex. This phenomenon is caused by the indoor air-CO_2 mixture density difference due to the combined effect of temperature and concentration. These effect assistant the fluid-flow to more accelerated movement. The highest velocity is on the vertical walls, and the lower values on the central vertical. The velocity of the room increases by the same factor as the Ra_T number increases.

Compared with the snapshots of temperature and concentration under different Ra_T, thermal convection becomes the dominant heat transfer mode with Ra_T increase. The heat and mass transfer at low thermal Rayleigh number ($Ra_T = 1 \cdot 10^4$) is mainly realized by bottom heating and heat conduction of indoor air-CO_2 mixture fluid. The heat and mass is transferred along the floor to the central area in room, with heat and mass conduction as the preponderant and low efficiency. Two-stages are exhibited for indoor mobility development. At the early stage, the heat and mass is transferred vertically through the floor, the temperature and concentration increase along the vertical direction the top, the isotherms and iso concentration-lines are almost horizontally distributed and paralleled, and the temperature lines and concentration-lines are stratified. At the later stage, the bottom heating stream is filled integrally into the top area of the room in the form of air mass. With the increase of Ra_T, the convection becomes dominant gradually, causing the increase of the flow velocity and the increase of the heat and mass transfer efficiency, which indicates that the heat and mass transfer is very rapid in this order. The temperature and concentration boundary-layer are formed on both sides of the wall due to the constant temperature and concentration of the sidewalls, eventually forming a convection cycle of the indoor air. The temperature and concentration boundary-layer is generated on the bottom side, heat and mass are transferred to the top area through the boundary-layer flow and diffuses evenly to the top area, and the isotherm and iso concentration-lines are no longer strictly kept horizontally distributed parallel to the bottom wall.

The influence of buoyancy ratio

The buoyancy ratio is an important parameter on the DDC problem, whose magnitude represents the relative magnitude of two driving forces. The analysis of buoyancy ratio is particularly important when the two driving forces are not simply counteracting or synergistic. In this case, whether the macroscopic transport structure of the DDC is dominated by the thermal buoyancy or by the concentration buoyancy or controlled by both depends on the specific value of buoyancy ratio.

Figure 6 shows the isotherms, iso concentrations and streamlines of opposing flow for $-5.0 \le N \le -0.1$ at $Ra_T = 10^7$, Pr = 0.7. The movement of the indoor flow was chaotic and varied dramatically at the start stage. The velocity on the left and right walls was much larger than that of the centre of the room, as shown in fig. 6 for the case $N = -1.0$, with minimum velocity located in the centre of the room. The indoor air-flow was a double vortex structure, which flows counterclockwise on the left and clockwise on the right along the horizontal centre and the horizontal central axis. It found that when $-5.0 \le N \le -1.0$, the thermal buoyancy force

is less than the concentration buoyancy force. The indoor flow movement is induced by natural convection under only the effect concentration, and the concentration buoyancy force weakens the thermal one as the negative buoyance ratio increase, leading to the more significant velocity. From fig. 6, it was also found that temperature and CO_2 concentration gradually decrease from floor to roof along the horizontal central axis, is homogeneous without stratification on the centre, lowest temperature and CO_2 concentration located on the upper and lower near the vertical walls. There are two stagnant zones. As for the case $N > -1.0$, the thermal buoyancy force is greater than the concentration buoyancy force. The movement of the indoor flow is derived by natural convection under only the effect temperature, and the CO_2 concentration buoyancy force weakens the thermal one as the negative buoyance ratio increase, leading to a smaller velocity. It is also observed that the isotherms and iso concentrations were linearly stratifications, which were sparse in part and dense in the lower part. The smaller distance of the isotherms lines and iso concentrations lines decreases with negative buoyancy ratio.

With the development of flow, the thermal boundary-layer is gradually formed along the bottom, and the bottom air-flows upward when heated, the top air-flows downward when cooled, and the symmetrically distributed thermal boundary-layer flow is formed inside left and right in room. Correspondingly, temperature change happens on the vertical walls of the room,

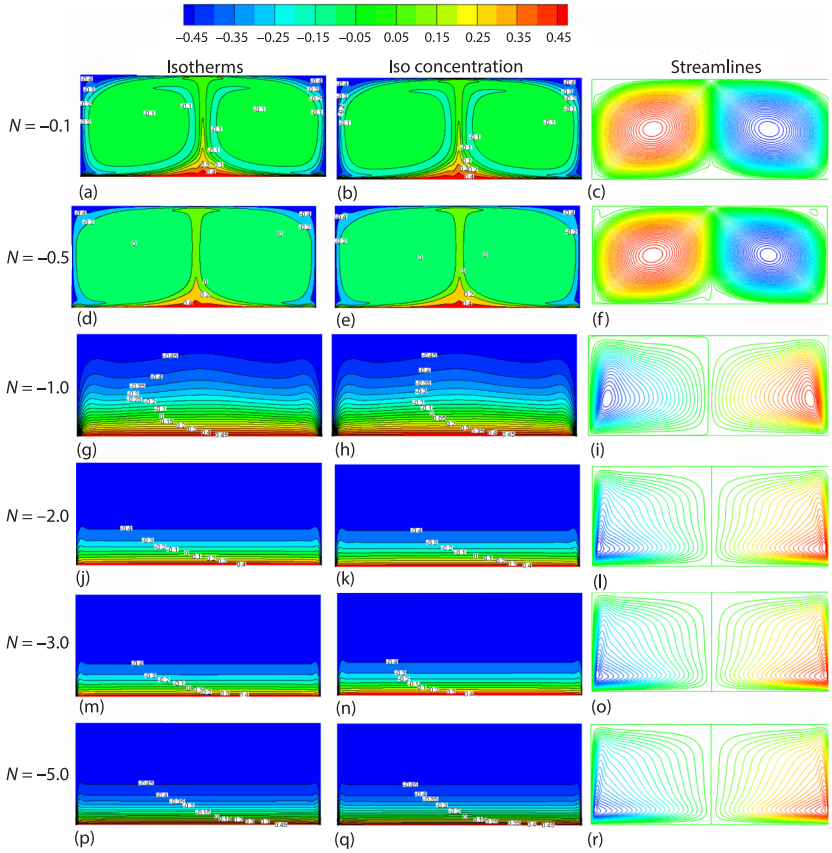

Figure 6. Dimensionless isothermal (a), (d), (g), (j), (m), and (p), iso-concentrations (b), (e), (h), (k), (n), and (q), and streamlines (c), (f), (i), (l), (o), and (r) varying at different N

the temperature drop on both sides of the pool is small because it is located at the bottom of upper convection, whose temperature is similar to the ambient temperature, with small temperature difference between them, so the wall heat dissipation caused by temperature difference is small, causing unapparent temperature decrease. The temperature in the bottom area increases gradually under the action of heat flow, and the temperature in the top area decreases gradually under the action of cold flow. With the continuous development of natural convection, heat is transferred to the core area on both sides of the room through the development of boundary-layer flow. When the flow develops completely, the indoor air forms temperature lines and concentration-lines stratification, the vertical temperature profile is stratified accordingly, and the vertical temperature gradient remains basically constant in the middle area of the indoor. The presence of CO_2 concentrations is sufficient to suppress indoor unstable convection.

Figure 7 shows the isotherms, iso concentrations and streamlines of aiding flow for $0.1 \leq N \leq 5.0$, at $Ra_T = 10^7$, Pr = 0.71, Le = 1.0. It can be seen that indoor air-flow movement was a double vortex structure, which flows counterclockwise on the left and clockwise on the right along the horizontal centre and central axis. It found that when $0.1 \leq N \leq 1.0$, the thermal buoyancy force is more significant than the concentration buoyancy force, and the indoor air-flow is driven by thermal natural convection. The concentration gradient becomes smaller, and the temperature gradient larger, leading to indoor air velocity lower with the

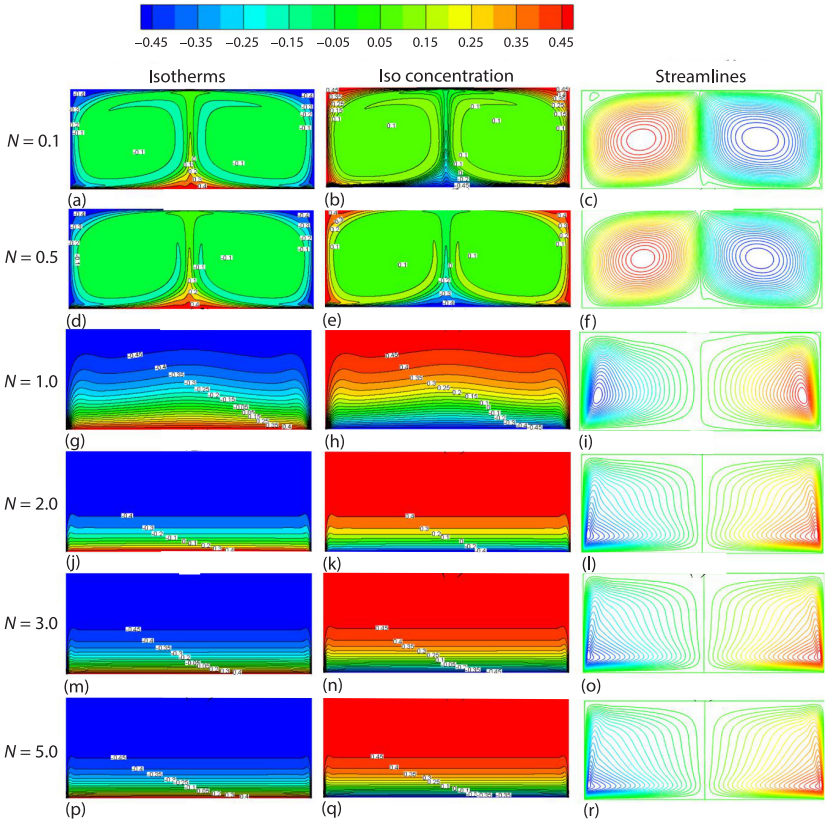

Figure 7. Dimensionless isothermal (a), (d), (g), (j), (m), and (p), iso-concentrations (b), (e), (h), (k), (n), and (q), and streamlines (c), (f), (i), (l), (o), and (r) varying at different *N*

buoyancy ratio increases. The highest temperature is located in the centre of the bottom wall. However, the highest CO_2 concentration is located on the left and right roof, and temperature and CO_2 concentration in the centre of the room is a more uniform distribution. When $N > 1.0$, the solutal buoyancy force is greater than the temperature buoyancy force, and the solutal buoyancy force induces the movement of the air-CO_2 mixture. It expect that due to the more extensive the buoyancy ratio is, the reinforcer, the concentration buoyancy is, and the movement of the fluid is accelerated. The isotherms are similar to the buoyancy ratio $N < 0$, with the highest temperature on the bottom wall and the lowest on the roof. Temperature stratification stays stable. The lower dense, the upper sparse. However, the iso-concentrations are opposite to the buoyancy ratio is negative, with the lowest concentration located on the bottom wall and the highest on the top roof. All these demonstrate that heat transfer is reinforced in the aiding flow and the time to reach a stable state is pronounced.

When the thermal Rayleigh number is small ($Ra_T = 1.0 \cdot 10^4$), the flow is mainly caused by heat conduction between the bottom hot wall and the surrounding cold wall, in which case the isotherm is almost vertical. The heat transfer mechanism gradually changes from conduction-dominated to convective-dominated, and the isotherm gradually becomes horizontal in the center of the chamber and remains vertical as Ra_T increase. However, it is formed when the two buoyancy forces of heat and mass are the same magnitude ($N = 1$) in the presence of concentration. At this time, the two buoyant forces of thermal and mass are in a state of mutual confrontation, and both sides are evenly matched. The two buoyancy forces control natural convection equally, causing non-uniform transmission structure in the close cavity, forming two large vortex structures on the left and right, which occupy most of the indoor space. The left vortex is counterclockwise and the right is clockwise. In this case, the heat and mass transfer path is more complicated. The left and right vortices cause heat and mass transfer path obstructed due to the unco-ordinated flow structure. Part of the heat and CO_2 remains on the left and right walls of the room as the two vortices rotate, and part of the heat flows along the lower part of the left vortex to the upper part of the right vortex and then transfers to the right wall of the cavity, and part of the CO_2 is transferred to the left wall along the right side of the left vortex in counterclockwise direction.

Heat and mass transfer

The Nu_m for different N at $Ra_T = 7.0 \cdot 10^6$ and $Ra_T = 1.0 \cdot 10^6$ which are calculated at the bottom wall as shown in fig. 8(a). When $N = -1.0$, the temperature and concentration buoyancy are forced to cancel each other, so the Nu_m reaches a minimum value, indicating that the heat and mass transfer efficiency is the lowest. When the concentration buoyancy force drives $N < -1.0$, the movement of the indoor fluid, Nu_m decreases linearly with the increase for each Ra_T, indicating that heat and mass transfer decrease as buoyancy ratio, N, increase. When $N > 0$, temperature and concentration buoyancy forces are cooperative. For each Ra_T, Nu_m increases linearly with the N increase, indicating that heat and mass transfer increase as the N increases. It is also noticed that Nu_m is symmetric regarding the axis $N = -1.0$. From fig. 8(b), it is seen that Nu_m increases as Ra_T increases. It is also shown that increasing Ra_T can improve the rate of heat and mass transfer.

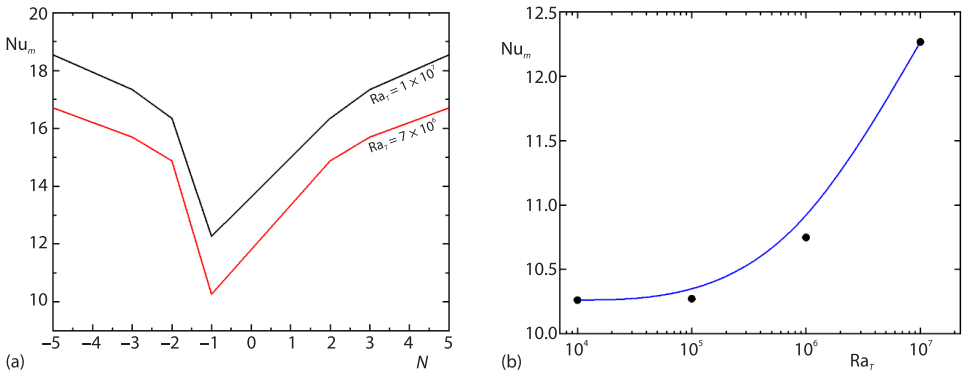

Figure 8. Heat and mass transfer Nu_m at different; (a) N and (b) Ra_T

Conclusions

The heat and mass transportation process of complex indoor fluid is to simulate indoor air-flow behavior and understand its basic characteristics, which is the main way and theoretical basis to control and regulate the indoor environment of buildings. Thermal buoyancy is the buoyancy force produced by fluids (gases or liquids) in some local regions of the flow field due to temperature differences from that of the fluid in the surrounding region. Under the action of buoyancy, the fluid with high temperature will rise and the fluid with low temperature will fall, thus forming convective flow in the flow field, and realizing the exchange and transfer of heat and mass through the heat exchange and mixing of convective flow. At present, the simulation of indoor air environment takes into account the driving effect of heat source buoyancy on indoor air-flow, while the influence of indoor pollutant differential concentration on indoor air-flow is not much. Although the influence of the former is more obvious than that of the latter, the indoor pollutant concentration has seriously exceeded the standard in recent years and has become an important threat to human health. The influence of contaminant differential concentration on indoor air-flow cannot be ignored.

The transient behaviour of thermosolutal DDC in a closed floor heating room filled with air-CO_2 mixture was studied using DNS over $1.0 \cdot 10^4 \leq Ra_T \leq 2.0 \cdot 10^7$, and $-5.0 \leq N \leq 5.0$. The results show that Ra_T significantly influences indoor air movement, heat, and mass transfer. Indoor air velocity increases, mass and heat transfer enhancement when Ra_T increases, as the combined buoyancy combined the effect of temperature and concentration is strengthened. The results also show that a positive buoyancy ratio significantly enhance mass and heat transfers and accelerates indoor air-flow, and the effect of temperature and concentration buoyancy forces are cooperative, and Nu_m increases when buoyancy ratio increase, improving the heat and mass transfer. Furthermore, when $-1 < N < 0$, the effect of temperature and concentration buoyancy are opposed, and air movement is driven by thermal buoyancy. When $N = -1$, the mass and heat transfer roughly cancel each other.

With the increase of Ra_T, the flow in the heating floor in close cavity increases gradually, eventually forming fluctuation of flow in room. At low thermal Ra_T, fluid viscosity is significant, with slow flow development, clear indoor temperature and concentration stratification, and smooth and evenly changed curve. Natural convection at high Ra_T develops rapidly, longitudinal slope of curve changes greatly, and local irregularity fluctuates along longitudinal direction. It indicates that when Ra_T increases, natural convection becomes intense, transient characteristics are more obvious, and turbulence instability occurs.

Nomenclature

A – aspect ratio
C – concentration, [%]
C_a – ambient concentration, [%]
C_H – highest concentration, [%]
C_L – lowest concentration, [%]
C_0 – reference concentration, [%]
D – mass diffusivity coefficient, [m^2s^{-1}]
g – gravitational acceleration, [m^2s^{-1}]
Le – Lewis number
N – buoyancy ratio
Nu_L – local nusselt number
Nu_m – average Nusselt number
P – pressure, [Pa]
Pr – prandtl number
p – dimensionless pressure, [–]
Ra_T – thermal Rayleigh number
Sc – Schmidt Number
T – temperature, [K]
T_a – temperature of the ambient fluid, [K]
T_H – highest temperature, [K]
T_L – lowest temperature, [K]
T_0 – reference temperature, [K]
t – time, [second]
U – velocity along the X-direction, [ms^{-1}]
u – dimensionless velocity in X-direction, [–]
v – dimensionless velocity in Y-direction, [–]

Greek symbols

α – thermal diffusivity, [m^2s^{-1}]
βC – concentration expansion coefficient, [$\%^{-1}$]
β_T – thermal expansion coefficient, [K^{-1}]
θ – dimensionless temperature, [–]
κ – thermal diffusivity of fluid, [m^2s^{-1}]
μ – absolute viscosity of fluid, [$kg(m/s)^{-1}$]
ρ – density, [kgm^{-3}]
ρ_a – density of the ambient fluid, [kgm^{-3}]
ν – kinematic viscosity of fluid, [m^2s^{-1}]
τ – dimensionless time, [–]
ϕ – dimensionless concentration, [–]

Acronyms

DDC – double diffusive convection
DNS – direct numerical simulation
FDM – finite different method
FVM – finite volume method
FEM – finite element method
LBM – lattice Boltzmann method
LES – large eddy simulation
MHD – magneto hydro dynamic

References

[1] Dadonau, M., *et al*., The Effect of Double Diffusion on the Dynamics of Horizontal Turbulent Thermohaline Jets, *Journal of Fluid Mechanics*, *905* (2020), A23, pp. 1-20
[2] Hunt, G. R., *et al*., Fountains in Industry and Nature, *Annual Review of Fluid Mechanics*, *47* (2015), 1, pp. 195-220
[3] Ostrach, S., Natural-Convection with Combined Driving Forces, *Physicochem-Ical Hydrodynamics*, *1* (1980), 4, pp. 233-247
[4] Goyeau, B., *et al*., Numerical Study of Double-Diffusive Natural-Convection in a Porous Cavity Using the Darcy-Brinkman Formulation, *International Journal of Heat and Mass Transfer*, *39* (1996), 7, pp. 1363-1378
[5] Ha, S. H., *et al*., Heat Transfer Study of Double Diffusive Natural Convec-Tion in A 2-D Enclosure at Different Aspect Ratios and Thermal Grashof Number During the Physical Vapor Transport of Mercurous Bromide (HG 2 br 2) – Part I: Heat Transfer, *Journal of the Korean Crystal Growth and Crystal Technology*, *32* (2022), 1, pp. 16-24
[6] Hao, Y., *et al*., Double-Diffusive Natural-Convection in a Nuclear Waste Repository, *Nuclear technology*, *163* (2008), 1, pp. 38-46
[7] Serrano-Arellano, J., *et al*., Heat and Mass Transfer by Natural-Convection in a Square Cavity Filled with a Mixture of Air-CO_2, *International Journal of Heat and Mass Transfer*, *64* (2013), Sept., pp. 725-734
[8] Beghein, C., *et al*., Numerical Study of Double-Diffusive Natural-Convection in a Square Cavity, *International Journal of Heat and Mass Transfer*, *35* (1992), 4, pp. 833-846
[9] Kamotani, Y., *et al*., Experimental study of Natural-Convection in Shallow Enclosures with Horizontal Temperature and Concentration Gradients, *International Journal of Heat and Mass Transfer*, *28* (1985), 1, pp. 165-173
[10] Koufi, L ., *et al*., Double-Diffusive Natural Convec-Tion in a Mixture-Filled Cavity with Walls' Opposite Temperatures and Concentrations, *Heat Transfer Engineering*, *40* (2019), 15, pp. 1268-1285
[11] Lee, J. W., *et al.*, Double Diffusive Convection in a Cavity under a Vertical Solutal Gradient and a Horizontal Temperature Gradient, *International Journal of Heat and Mass Transfer*, *34* (1991), 9, pp. 2423-2427
[12] Lee, J., *et al*., Confined Natural-Convection Due to Lateral Heat-Ing in a Stably Stratified Solution, *International Journal of Heat and Mass Transfer*, *33* (1990), 5, pp. 869-875

[13] Chen, S., *et al*., Numerical Investigation of Double-Diffusive (Natural) Convection in Vertical Annuluses with Opposing Temperature and Concentration Gradients, *International Journal of Heat and Fluid-Flow*, *31* (2010), 2, pp. 217-226
[14] Corcione, M., *et al.*, Correlations for the Double-Diffusive Natural-Convection in Square Enclosures Induced by Opposite Tem-Perature and Concentration Gradients, *International Journal of Heat and Mass Transfer*, *81* (2015), Feb., pp. 811-819
[15] Xu, H., *et al.*, Lattice Boltzmann Simulations of the Double-Diffusive Natural-Convection and Oscillation Characteristics in an Enclosure with Soret and Dufour Effects, *International Journal of Thermal Sciences*, *136* (2019), Feb, pp. 159-171
[16] Xu, H., *et al.*, Lattice Boltzmann Simulation of The Double Diffusive Natural-Convection and Oscillation Characteristics in an Enclosure Filled with Porous Medium, *International Communications in Heat and Mass Transfer*, *81* (2017), Feb., pp. 104-115
[17] Nia, M. F., *et a*l., Thermohydrodynamic Characteristics of Combined Double-Diffusive Radiation Convection Heat Transfer in a Cavity, *Comptes Rendus Mecanique*, *347* (2019), 5, pp. 406-422
[18] Liang,Y., *et al.*, The Effect of Rotation on Double Diffusive Convection: Perspectives from Linear Stability Analysis, *Journal of Physical Oceanography*, *51* (2021), 11, pp. 3335-3346
[19] Abed Meften, G., *et al*., Non-Linear Stability and Linear Instability of Double-Diffusive Convection in a Rotating with Ltne Effects and Symmetric Properties: Brinkmann-Forchheimer Model, *Symmetry*, *14* (2022), 3, pp. 1-13
[20] Shankar, B. M., *et al*., Stability of Double-Diffusive Natural-Convection in a Vertical Fluid Layer, *Physics of Fluids*, *33* (2021), 9, pp. 87-105
[21] Kumar, S., *et al.*, Double-Diffusive Convection in a Rectangu-Lar Cavity Subjected to an External Magnetic Field with Heated Rectangu-Lar Blockage Insertion for Liquid Sodium-Potassium Alloy, *Physics of Fluids*, *34* (2022), 2, 023604
[22] Parveen, R., *et al*., Heat and Mass Source Effect on Mhd Double-Diffusive Mixed Convection and Entropy Generation in a Curved Enclosure Filled With Nanofluid, Non-Linear Analysis, *Modelling and Control*, *27* (2022), 2, pp. 308-330
[23] Hussain, S., *et al*., Impact of Magnetic Field and Entropy Generation of Casson Fluid on Double Diffusive Natural-Convection in Staggered Cavity, *International Communications in Heat and Mass Transfer*, *127* (2021), 105520
[24] Ali, A. H., *et al*., A Study of Continuous Dependence and Symmetric Properties of Double Diffusive Convection, Forchheimer Model, *Symmetry*, *14* (2022), 4, pp. 1-18
[25] Meften G., Ali A., Continuous Dependence for Double Diffusive Convection in a Brinkman Model with Variable Viscosity, Acta Universitatis Sapientiae, *Mathematica*, *14* (2022), 1, pp. 125-146
[26] Chen, S., *et al.*, Numerical Study of Turbulent Double-Diffusive Natural-Convection in a Square Cavity by Les-Based Lattice Boltzmann Model, *International Journal of Heat and Mass Transfer*, *55* (2012), 17-18, pp. 4862-4870
[27] Chen, S., *et al*., Double Diffusion Natural-Convection in a Square Cavity Filled with Nanofluid, *International Journal of Heat and Mass Transfer*, 95 (2016), Apr., 1070-1083
[28] Wang, J., *et al*., Onset of Double-Diffusive Convection in Horizontal Cavity with Soret and Dufour Effects, *International Journal of Heat and Mass Transfer*, *78* (2014), Nov., pp. 1023-1031
[29] Nee, A., Hybrid Lattice Boltzmann Simulation of 3-D Natural-Convection, *Journal of Computational and Theoretical Transport*, *50* (2021), 4, pp. 280-296
[30] Carpenter, J., *et al*., Stability of a Double-Diffusive Interface in the Diffusive Convection Regime, *Journal of physical oceanography*, *42* (2012), 5, pp. 840-854
[31] Liang, X., *et al*., Complex Transition of Double-Diffusive Convection in a Rectangular Enclosure with Height To-Length Ratio Equal to 4 – Part I, *Communications in Computational Physics*, *6* (2009), 2, 247
[32] Penney, J., *et al*., Direct Numerical Simulation of Double-Diffusive Gravity Currents, *Physics of Fluids*, *28* (2016), 8, 086602
[33] Serrano-Arellano, J., *et al*., Numerical Investigation of Transient Heat and Mass Transfer by Natural-Convection in a Ventilated Cavity: Outlet Air Gap Located Close to Heat Source, *International Journal of Heat and Mass Transfer*, *76* (2014), Sept., pp. 268-278
[34] Serrano-Arellano, J., *et al.*, Conjugate Heat and Mass Transfer by Natural-Convection in a Square Cavity Filled with a Mixture of Air-CO_2, *International Journal of Heat and Mass Transfer*, *70* (2014), Mar., pp. 103-113
[35] Nikbakhti, R., *et a*l., Double-Diffusive Natural-Convection in a Rect-Angular Cavity with Partially Thermally Active Side Walls, *Journal of the Taiwan Institute of Chemical Engineers*, *43* (2012), 4, pp. 535-541

[36] Nikbakhti, R., *et al*., Numerical Investigation of Double Diffusive Buoyancy Forces Induced Natural-Convection in a Cavity Partially Heated and Cooled from Sidewalls, *Engineering Science and Technology, an International Journal*, *19* (2016),1, pp. 322-337
[37] Benbrik, A., *et al*., In teraction of Radiation with Double-Diffusive Natural-Convection in a 3-D Cubic Cavity Filled with a Non-Gray Gas Mixture in er-Ating Cases, Numerical Heat Transfer – Part A: Application, *International Journal of Computation and Methodology*, *69* (2016), 1/6, pp. 479-496
[38] lhusseny, A., *et al*., A Numerical Study of Double-Diffusive Flow in a Long Rotating Porous Channel, *Heat and Mass Transfer*, *51* (2015), 4, pp. 497-505
[39] Khalaf, H. I., *et al*., Double-Diffusive Air-CO_2 Mixture Flow in A Staggered Cavity with Numerous Concave Lower Wall Aspect Ratios, *The European Physical Journal Plus*, *136* (2021), 5, pp. 1-20
[40] Oosthuizen, P. H., *et al*., *An Introduction Convective Heat Transfer Analysis*, MC-Graw Hill, New York, USA, 1999
[41] Sezai, I., *et al*., Double Diffusive Convection in a Cubic Enclosure with Opposing Temperature and Concentration Gradients, *Physics of Fluids*, *12* (2000), 9, pp. 2210-2223
[42] Xam'an, J., *et al*., Optimum Ventilation Based on the Overall Ventilation Effectiveness for Temperature Distribution in Ventilated Cavities, *International Journal of Thermal Sciences*, *48* (2009), 8, pp. 1574-1585

Paper submitted: November 7, 2022
Paper revised: January 13, 2023
Paper accepted: February 15, 2023